Title
Facile Decomposition of Organophosphonates by Dual Lewis Sites on a Fe3O4(111) Film

Journal
JOURNAL OF PHYSICAL CHEMISTRY C, 124(23)

ISSN
1932-7447

Authors
Walenta, Constantin A
Xu, Fang
Tesvara, Celine
et al.

Publication Date
2020-06-11

DOI
10.1021/acs.jpcc.0c01708

Facile Decomposition of Organophosphonates by Dual Lewis Sites on a Fe_3O_4(111) Film

Constantin A. Walenta[a], Fang Xu[a], Celine Tesvara[b], Christopher R. O'Connor[a], Philippe Sautet[b,c], Cynthia M. Friend*[,a,d]

[a]Department of Chemistry & Chemical Biology, Harvard University, Cambridge, MA 02138, USA
[b] Chemical and Biomolecular Engineering Department, University of California, Los Angeles, Los Angeles, CA 90095, USA
[c] Chemistry and Biochemistry Department, University of California, Los Angeles, Los Angeles, CA 90095, USA
[d]John A. Paulson School of Engineering and Applied Sciences, Harvard University, Cambridge, MA 02138, USA

Corresponding Author: friend@fas.harvard.edu

Abstract

Dimethyl methylphosphonate (DMMP) is used as a simulant for toxic nerve agents and pesticides, rendering understanding of surface chemistry requisite to design effective materials for organophosphonate (catalytic) decomposition at room temperature. In this work, DMMP surface chemistry is studied on a iron oxide surface in a very well-defined environment using temperature programmed reaction, isotopic labelling, scanning tunneling microscopy, X-ray photoelectron spectroscopy and density functional theory. DMMP, $(CH_3O)_2P(O)(CH_3)$, dissociates to yield methoxy and methyl methyl phosphonate, $(CH_3O)P(O)_2(CH_3)$, on the surface at room temperature. At higher temperatures, dimethyl ether forms via intramolecular reaction, followed by formation of formaldehyde and methanol from adsorbed methoxy decomposition during temperature programmed reaction. Ultimately, stochiometric combustion at 870 K produces CO, $H_2C=O$, CO_2 via reaction with lattice oxygen; with PO_x remaining on the surface. Excess oxygen from the bulk is required to drive these higher temperature pathways. Neither hydrolysis, nor a photoreaction is observed, when exposing the adsorbed DMMP to water or light above the bandgap, respectively. No evolution of P-containing species is detected, indicating efficient trapping of this contaminant. The activity for DMMP decomposition at room temperature is reduced by the accumulation of PO_x. However, a significant amount of reaction persists after multiple temperature programmed reaction experiments.

Introduction

Organophosphonates are compounds that are often extremely toxic, rendering their destruction important for a healthy environment. Ideally, such toxins could be catalytically decomposed at room temperature. This is especially the case for organophosphonates that are used as chemical warfare agents (CWAs) because they are released under ambient conditions.[1] Dimethyl methylphosphonate (DMMP) is often used as a model for one common and highly toxic agent, sarin;[1-2] thus providing insight

into the elementary steps that can lead to decomposition. Additionally, the environmental chemistry of organophosphonates[3] including DMMP is of broad interest because many pesticides are based on the organophosphonate structural motif[2], including the controversial, potentially carcinogenic glyphosate.[4-5] Potential materials to decompose organophosphonates should be non-toxic, exhibit a high surface area and be earth abundant. Iron oxides are promising materials that meet the desired specifications, but studies of organic compounds in very well-defined environments are limited.[6]

Metal oxides have potential for room temperature decomposition of toxic organophosphonates. Indeed, the surface chemistry of oxides of Fe[7-13], Cu[14-15], Y[16], Mo[17] , Ti[18-20], Zn[21] and others[22-24] has been investigated. A common DMMP reaction pathway for the studied oxides is the dissociation of one of the P-O-CH_3 bonds and the formation of a surface methoxy[15-16, 18, 20] or molecular methanol in the presence of surface hydroxyls.[7, 21] While the exact decomposition temperature of DMMP on the oxides differs slightly, iron oxides activate also the P-CH_3 bond above room temperature.[25] This reaction pathway is attributed the reducibility of the Lewis acid iron surface sites, but the reaction mechanism remains elusive.[25] Understanding the surface chemistry and reaction mechanisms of CWA stimulants such as DMMP on the bare oxide is essential to improve agent trapping and decomposition reactions at room temperature.

Herein, the efficient decomposition of DMMP at room temperature on a Fe_3O_4(111) (magnetite) thin film supported on Fe_2O_3(0001) (hematite) is demonstrated. This surface was selected because it has dual Lewis acid and base sites, where the Oxygen adatoms as Lewis acid sites may bind to the P of the DMMP and the Fe-sites as Lewis base sites accept nucleophils like methoxy species to yield an efficient decomposition process. Furthermore, based on prior work, there is an atomic level understanding of the surface reactivity towards methanol and methoxy.[26] At 300 K, DMMP irreversibly reacts, yielding adsorbed methoxy species and methyl methylphosponate species. There are three decomposition pathways that yield organic products above 600 K. Excess oxygen from the bulk drives loss of methoxy and methyl and oxidation of the phosphorous. No P-containing products leave the surface up to 900 K; thus, eliminating the toxic phosphonate group from the gas phase. The accumulation of P-containing products diminishes further DMMP decomposition, so the process is not catalytic.

Methods

Experimental

The reactivity measurements were carried out in an ultrahigh vacuum (UHV) apparatus with a base pressure of < 8×10^{-11} Torr, which has been described in detail before.[27-28] The α-Fe_2O_3(0001) single crystal (SurfaceNet GmbH) is mounted as described previously and the sample temperature can be controlled between 130 K and 1000

K.[28] Crystal cleaning is accomplished by Ar^+-ion sputtering (1.0 keV, 1.0×10^{-5} Torr, 15 min, 13 μA sample current) and annealing in vacuo (1000 K, 15 min). Before every experiment, 3 cycles of sputtering and annealing are performed to remove all potential contaminants. The reductive sample preparation is known to result in a Fe_3O_4(111) surface termination, that has been thoroughly characterized.[26, 28-30] The surface ordering is confirmed by low energy electron diffraction (see Fig. S1). For the sake of readability, this surface is labelled Fe_3O_4(111)-terminated surface throughout the manuscript.

Dimethyl methylphosphonate (DMMP) (≥97%, Sigma-Aldrich) was further purified by several pump-freeze cycles. To avoid potential hydrolysis in the dosing system, the gas line system was passivated with 1 h of DMMP exposure[31] and further flushed and pumped several times. DMMP adsorption was performed with a pressure of 1.0×10^{-9} Torr at room temperature, unless otherwise stated. An exposure of 60 s at room temperature is equivalent to a saturation dose. All given pressures and exposures do not account for an enhancement factor of the needle doser, that was determined to be 27 previously. Isotopically labelled methanol-d_3 (CD_3OH, 99.8 atom% D, Sigma-Aldrich) was dosed with a separate needle doser to avoid any hydrolysis of DMMP during the exposures. Water (VWR, HPLC grade) was dosed via a completely separated gas dosing system.

Temperature-programmed desorption and reaction measurements were performed with the crystal in line-of-sight of the quadrupole mass spectrometer with a constant heating rate of 1 K/s. The masses monitored were m/e 2, 15, 16, 18, 27, 28, 29, 30, 31, 32, 33, 35, 44, 46, 47, 79, 124. The gaseous products were identified by their fragmentation patterns and quantified by correcting for mass spectrometer sensitivity the ionization cross sections. The used ionization cross section values are summarized in Table S1.[32-34] Illumination for photochemical experiments was carried out with a 300 W Xe lamp with a short pass filter at 400 nm (3.1 eV, Asahi Spectra), well above the indirect band gap of 2.2 eV[35] and the direct optical band gap of 2.7 eV for hematite.[6] The flux was measured to be 9.8 mW/cm^2 and 15% of this flux had wavelengths higher than 400 nm.

Scanning Tunneling Microscopy (STM) was performed in a commercial Omicron VT Beam Deflection AFM/STM system as described previously.[28, 36] The single crystal was mounted on a standard flag-style single layer sample plate and a Pt-Ir tip was used for the STM experiments. The same set of preparation cycles lead to a clean and flat Fe_3O_4(111)/Fe_2O_3(0001) surface as evidenced by LEED and STM images.

X-ray photoelectron spectroscopy (XPS) experiments were performed at the Center of Functional Nanomaterials, Brookhaven National Laboratory, in a commercial system from SPECS. The DMMP was exposed to the clean crystal in the STM system at Harvard and subsequently transferred to the setup at the Center for Functional Nanomaterials using an ultra-high vacuum suitcase. The XPS data were obtained using monochromatized Al K_α radiation (1486.7 eV) incident on the sample at 54.7°

with respect to the hemispherical analyzer. Photoelectrons were measured with normal emission using a pass energy of 50 eV. The calibration was performed by setting the Ag $3d_{5/2}$ peak to 368.2 eV of a reference Ag(111) single crystal. Each XP spectrum was first normalized by dividing by the average value of the low-energy side of the spectrum with a width of 1 eV. The background was subtracted by using a linear background for the P2p region and a Shirley background for the O1s and Fe2p region.[37] A Voigt line shape was used to fit the P2p and subtracted O1s spectra. The quantification of the P2p and O1s regions were performed by dividing the peak areas by the atomic sensitivity factors.[38]

Theory

Spin polarized DFT+U calculations were performed to study molecular and dissociative adsorption, as well as further decomposition of DMMP on the Fe_3O_4(111) surface. The calculations were performed using the Vienna ab initio simulation package (VASP)[39], with the projector augmented wave (PAW)[40] method employed to describe the electron-ion interactions. The Perdew-Burke-Ernzenhof (PBE)[41] exchange and correlation functional, within the generalized gradient approximation (GGA), was used alongside with the dDsC[42-43] dispersion correction to describe the Van der Waals contributions to the energy. The electronic energy was converged to 10^{-6} eV and Geometry optimization calculations follow an atomic force criterion of 0.03 eV/Å. The one electron wave function was expanded on a plane wave basis set with a cutoff energy of 500 eV for bulk and 400 eV for surfaces.

The surface model is based on an optimized bulk Fe_3O_4 crystal, with a cell consisting of 24 Fe and 32 O atoms. The bulk is cut to create a p(2x2) supercell of the stoichiometric Fe_3O_4 surface in the [111] orientation (Fig. S2) . The slabs are terminated by tetrahedrally-coordinated Fe and consist of 12 atomic layers (48 Fe and 64 O atoms).[44] The unit cell lattice vector is $\frac{a_0}{\sqrt{2}} = 11.921$ Å where each unit cell has 4 Fe tetrahedral atoms on the terminated surface. Each periodic slab is separated by a vacuum length of 20 Å (large vacuum employed to accommodate the size of DMMP for adsorption calculations). The lowest five atomic layers are kept frozen to mimic the bulk. Surfaces used in the DMMP decomposition chemistry calculations employs oxygen coverage of 1/4 ML following experimental observations (1 oxygen bonded to one of four termination Fe tetrahedral). The dipole-dipole interactions between repeated slabs in the z direction were compensated using the Makov-Payne method in addition to Harris correction to forces per VASP implementation.[45]

Due to the strong on-site Coulomb interaction occurring at d-orbitals of Fe, DFT+U correction was implemented with U = 4.50 eV and J = 0.89 eV (Ueff = 3.61 eV) following the correction method proposed by Dudarev et al.[46] This U value yields local magnetic moment value for tetrahedral and octahedral Fe ions -4.02 and 4.07 μ_B respectively which are in good agreement with previous published literature (4.05 μ_B).[47-48]

The integration over the Brillouin zone on bulk calculations were performed using a Monkhorst Pack[49] grid k-point mesh of 5x5x5. The optimized bulk structure yields lattice parameter a = 8.43Å. Surface calculations use Γ-point only. A test with a 3x3x1 k-point mesh shows that DMMP chemisorption energy only changes by 0.02 eV, justifying the Γ-point only approximation.

Results and Discussion

Tracking the DMMP Decomposition Mechanism

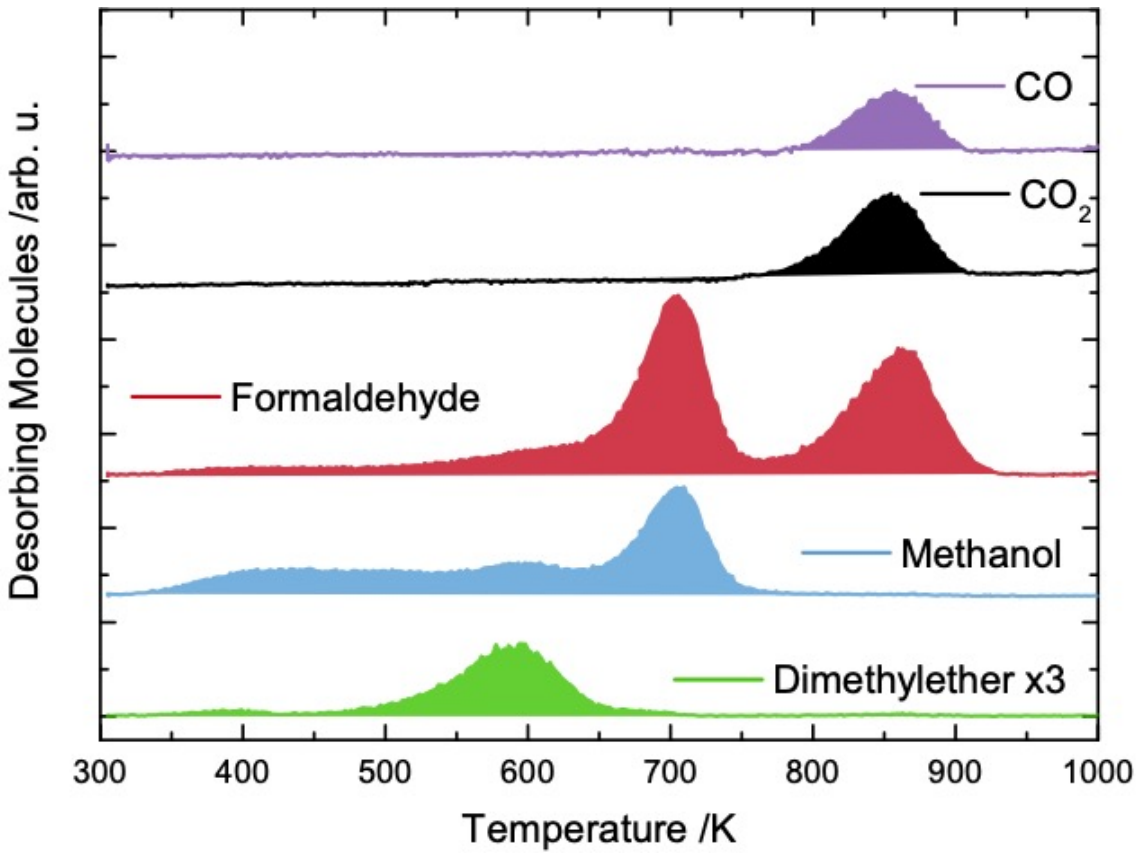

Fig. 1: Dimethyl methylphosphonate [$(CH_3O)_2(CH_3)PO$] decomposes to methanol, formaldehyde and dimethylether on $Fe_3O_4(111)/Fe_2O_3(0001)$ below 750 K in temperature programmed reaction experiments. CO and CO_2 are formed at ~870 K. No P-containing products are detected. The data were obtained after exposing the $Fe_3O_4(111)/Fe_2O_3(0001)$ surface to a saturation dose of DMMP (1.0×10^{-9} Torr, 1 min) at room temperature. The traces are offset for clarity and the features are colored to guide the eye. All data have been corrected for fragmentation and ionization cross sections as described in the experimental section. Methanol is tracked by mass 31, formaldehyde by mass 30, dimethylether by mass 46, and CO with mass 28 and CO_2 with 44.

The primary gas phase products of dimethyl methylphosphonate (DMMP) decomposition below 750 K are methanol and formaldehyde (Fig. 1). These reaction products are attributed to a disproportionation reaction of surface methoxy, based on prior studies of methanol on this surface.[26, 28] The peak temperature coincides exactly with the reaction temperature from pure methanol exposure on the $Fe_3O_4(111)$-

terminated surface.[26] Small amounts of methanol desorption are also observed between 350 K and 600 K, which are attributed to the reaction of surface-bound methoxy with surface hydroxyls bound to defects.

Molecularly adsorbed DMMP desorbs around 270 K and a DMMP multilayer sublimes at 190 K;[9] hence, no molecular desorption is observed at room temperature (Fig. S7 and S8a). At the room temperature saturation coverage, all DMMP molecules adsorb dissociatively and in analogy to work on ceria[22] and cupric oxide[14] the mechanism is attributed to a P-OCH_3 bond cleavage which leads to formation a surface methoxy species and methyl methylphosphonate (MMP).

Two thermodynamically stable isomeric conformations of molecularly chemisorbed DMMP were found by DFT on Fe_3O_4(111) (Fig. 2, Fig. S3, Table S2). In the model an oxygen coverage of ¼ monolayer (ML) is included to mimic the experimental surface, which has been previously shown to contain O adatoms.[26] Models of the relaxed geometries explored are given in the supporting information (Figure S3, Table S2). The most stable DMMP molecular adsorption configuration involves interaction of the oxygen of the phosphonate group (P=O) with a tetrahedral Fe on the surface, yielding an adsorption energy of -2.57 eV (Fig. 2A). An additional weak interaction occurs between one DMMP methoxy and the O-adatom on the surface. The $(P{=}O)_{DMMP}$---$(Fe_{tet})_{surf}$ bond length is 1.94 Å and the distance between C of methyl and O-adatom equals to 2.95 Å.

Dissociation of DMMP to adsorbed methoxy and a methyl-methylphosphonate (MMP) [$(CH_3O)(CH_3)P(O)(O_{surf})$] on the surface is thermodynamically favorable by 1.19 eV, based on DFT (Fig. 2B). Methoxy adsorbed alone on Fe_3O_4(111) (¼ ML O) is most stable on tetrahedral Fe sites, the Lewis base site. The site preference test on methoxy was done by performing dissociative methanol adsorption on a clean Fe_3O_4(111). This test yields a dissociative adsorption energy of methanol of -2.82 eV, which agrees well to previous published literature.[50] Subsequent investigation of possible adsorption modes of MMP in the presence of a single methoxy bonded on tetrahedral Fe yielded three possible adsorption conformations (Fig. S4 and Table S3). The most stable MMP adsorption conformation correspond to P interacting with an O adatom on the surface (Fig. 2B), yielding a total adsorption energy of -3.76 eV, referenced to gas phase DMMP. The, P-O_{adatom} distance is 1.56 Å and the oxygen of MMP P=O group faces the nearby adsorbed methoxy, creating a stabilization via van der Waals interaction. We postulate that the strong adsorption energy correlates with phosphonate re-establishing its 3 coordination with oxygen upon dissociation with methoxy. Other explored structures for MMP adsorption on surface Fe atoms are higher in energy and give a markedly endothermic dissociation. This shows that O adatoms, present on the surface, are key for the dissociation of DMMP.

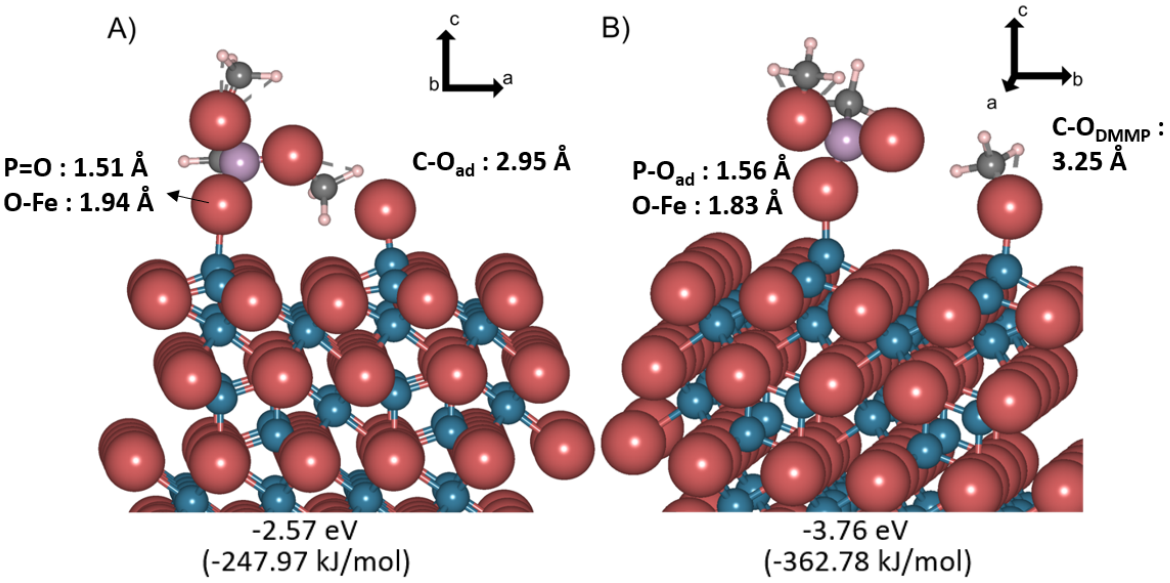

Fig. 2: Perspective views of the most stable configurations and their respective energies for (A) DMMP [$(CH_3O)_2(CH_3)PO$] adsorbed molecularly on $Fe_3O_4(111)$ with an oxygen adatom (-2.57 eV / -247.97 kJ/mol) and (B) MMP [$(CH_3O)(CH_3)P(O)(O_{surf})$] coadsorbed with a single methoxy bound to a tetrahedral iron lattice site (-3.76 eV / -362.78 kJ/mol). Dissociative adsorption is thermodynamically favored over molecular adsorption. Other adsorption configurations considered for molecular DMMP (Fig. S2 and Table S2) and dissociated DMMP are higher in energy (Fig. S3, Fig S4 and Table S3). Blue represents Fe atoms and red indicates oxygen atoms. Ionic radii are used in the representation.

Around 600 K, dimethyl ether as the first significant reaction product is formed MMP alone and that is does *not* involve adsorbed surface methoxy (Fig. 1). Dimethyl ether produced from DMMP has been reported on other oxides; however, the reaction mechanism was not previously determined.[7, 23] Here, isotopic labelling studies were used to identify the reaction pathway of dimethyl ether formation on the $Fe_3O_4(111)$-terminated surface (Fig. S8). Sequential exposure of the surface to DMMP and CD_3OH on the surface, yielded both adsorbed CD_3O and CH_3O, resulting from dissociation of CD_3OH and DMMP, respectively, based on the production of both deuterated and non-deuterated products, including $D_2C{=}O$ and $H_2C{=}O$, at ~700 K, the temperature characteristic of methoxy decomposition (Fig. S8). On the other hand, no deuterated dimethyl ethere is formed. A detailed analysis of the temperature programmed reaction data indicates that *only* $(CH_3)_2O$ is formed. Furthermore, no dimethyl either is dectected from reaction of methanol produced from methoxy. Hence, the formation of dimethyl ether must solely proceed via adsorbed MMP species, ***not*** from methyl transfer to a surface-bound methoxy species. The thermodynamics of this process are addressed in DFT calculations below.

Further decomposition of MMP and methoxy requires forther excess O to render the formation of dimethyl ether thermodynamically favorable (Fig 3). In the absence of another O-adatom, further cleavages of P-O or P-C bonds are not favorable or uphill by 1.38 eV (Fig S5). The additional oxygen leads to formation of a P-O bond, leading to a net thermodynamically downhill process (S5-S6). The oxygen adatom is created by the bulk reduction of the hematite (Fe_2O_3) substrate to magnetite (Fe_3O_4) and the chemical potential of this O atom was evaluated following this reaction. This presence of extra oxygen is in agreement with previous STM work showing a layer of oxygen adatoms forming upon heating.[26] Further details on the formation of DME from different intermediates can be found in the supporting material.

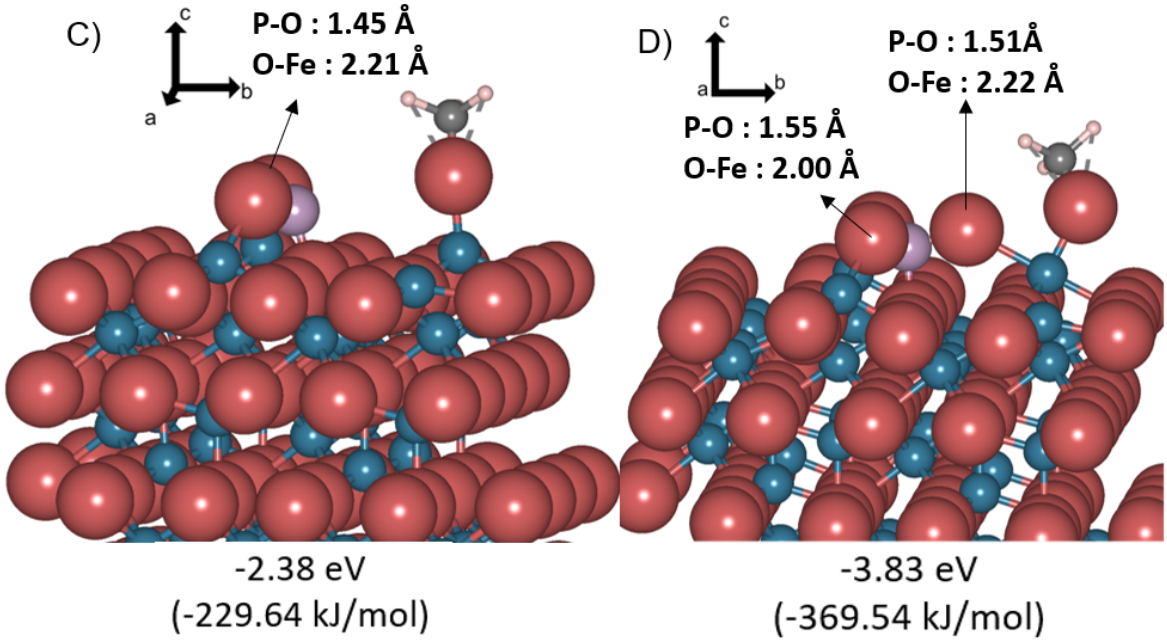

Fig. 3: Perspective views of POx structures formed after self rearrangement of MMP to produce DME, leaving the adsorbed methoxy on the surface, showing that an extra O adatom is required to make this transformation thermodynamically favorable. (C) Species formed with no excess O, having an energy of -2.38 eV / -229.64 kJ/mol, making it markedly less stable than MMP and methoxy (Fig. 2); and, (D) the stabilized POx species formed from reaction with an extra O-adatom, yielding an energy of -3.83 eV / -369.54 kJ/mol, which is slightly more stable than MMP plus methoxy (Fig 2B).

A third reaction channel is observed between 800 and 950 K, yielding formaldehyde, CO, CO_2 (Fig. 1) and H_2O (Fig. S8a). These products are attributed to the combustion of residual organic groups still bound to P.

The integrated molecular yields from DMMP temperature programmed reaction normalized to the amount of methanol confirms that all products are accounted for (Tables 1, S4). Dimethyl ether formation is a minor reaction pathway, while the methanol disproportionation is nearly stoichiometric within the experimental error, and about half of the products are combustion products above 800 K. Analysis of the stoichiometry of gaseous products (Table 1) reveals that the total amount of the

desorbed oxygenates is stoichiometric (Table S4) under the assumption that all the P-X (X = C, O) single bonds break during temperature programmed reaction in analogy to previous findings on metal oxides.[9, 51] The resulting PO_x-species is strongly adsorbed on the surface and could only be removed by sputtering. The stoichiometry analysis (Table S4) presents compelling evidence, that the mass balance for hydrogen, carbon and oxygen is closed in these experiments. Throughout all the reaction channels, phosphorous remains irreversibly bound to the surface and no other P-containing species is observed.

Table 1: Integrated amounts of desorbing molecules from a saturation dose of dimethyl methylphosphonate at 300 K on the Fe_3O_4(111)-terminated Fe_2O_3(0001) surface (Fig. 1).

Peak	600 K	700 K		870 K			
Molecule	$(CH_3)_2O$	CH_3OH	CH_2O	CH_2O	CO	CO_2	H_2O
Relative Amount [% of CH_3OH]	17	100	88	71	41	77	323

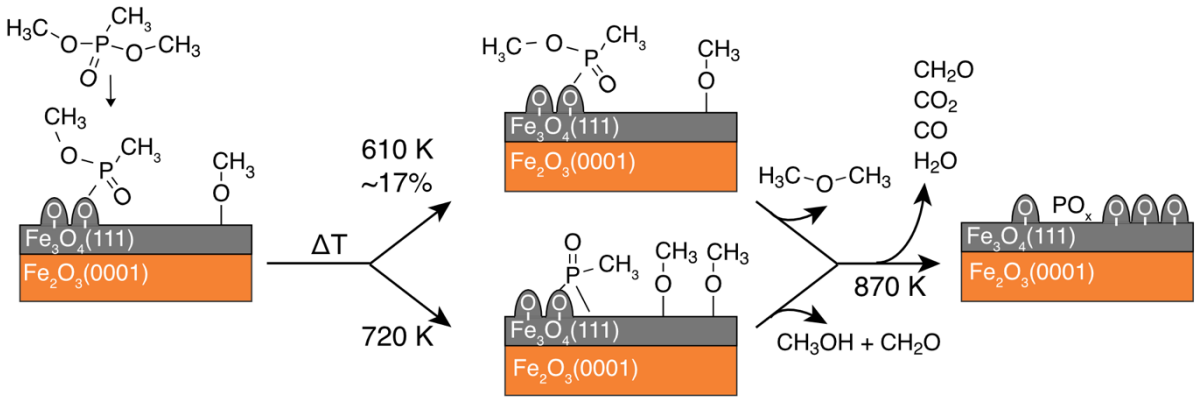

Scheme 1: Reaction Pathways of dimethyl methylphosphonate on Fe_3O_4(111) terminated Fe_2O_3(0001). At room temperature, DMMP dissociates to yield methoxy and methoxy methylphosphonate (MMP). Further reaction requires higher temperature to yield volatile oxygenates and adsorbed PO_x. The volatile products include dimethyl ether (17%) formed from intramolecular decomposition of surface-bound methylphosphonate (MP), and formaldehyde and methanol formed via reaction of adsorbed methoxy. Ultimately, residual P-bound hydrocarbons combust around 870 K via reaction with oxygen from the lattice. The PO_x-species remains irreversibly bound on the surface.

A summary of the observed reaction channels (Scheme 1) shows the two major oxidation pathways for DMMP on the surface. The dimethyl ether formation is a minor pathway and presumably an MMP species undergoes an internal rearrangement to yield dimethyl ether and a PO_x species. DFT shows that the remaining P species on the surface is stabilized by migration of an O atoms from the subsurface.

Simultaneously, methoxy abstraction from DMMP yields surface bound methoxy species, that decompose at 720 K to formaldehyde and methanol. At 870 K, the residual carbon containing species undergo oxidation and stoichiometric oxidation products CO, CO_2, CH_2O and H_2O are obtained. In this mechanism, desorption of P-containing species is not observed (Fig. S3a).

Scanning tunneling microscopy (STM) images show that the residual P-containing species form highly ordered islands after heating to 800 K to eliminate most carbon (Fig. 4). The image of as-prepared $Fe_3O_4(111)/Fe_2O_3(0001)$ surface also shows that the surface is terminated by a combination of close packed O_{ad}-atom structures with a coverage of 0.67 ML and exposed Fe-lattice sites, as we reported previously.[26] Based on modeling of the STM images using DFT, the dark regions are Fe centers and the bright features are O under the tunneling conditions used (Fig. 4A). At room temperature, the STM images after exposure of a saturation amount of DMMP are not as well resolved as the clean surface due to dynamic processes such as the diffusion of surface species. Nevertheless, the adsorbates at room temperature present a short-range ordered hexagonal pattern, the same as the $Fe_3O_4(111)$ termination.

After annealing the surface to 750 K, island formation is observed (Fig. 4C). The phosphorus-species related islands are well templated by the $Fe_3O_4(111)/Fe_2O_3(0001)$ substrate, as the comparison between islands and substrate indicates an on-top occupation with the same lattice constant.The residual surface species at 750 K most likely has a PO_3 stoichiometry based on X-ray photoelectron spectra that clearly show that P-containing species are present (Fig. S9-S12). Unfortunately, the signal-to-noise ratio prohibits a meaningful assignment of the complete chemical environment of the phosphorous species. The binding energies of the phosphorous peaks are 133.1 eV and 134.0 eV in good agreement with literature values.[17, 52-53] Comparison to data for phosphonate species, a 2.91 peak area ratio of O/P is obtained (Table S5), indicating a possible PO_3 surface adsorbate stoichiometry at an 750 K annealed surface, corroborating the proposed reaction mechanism (Scheme 1 and also Fig. 3B).

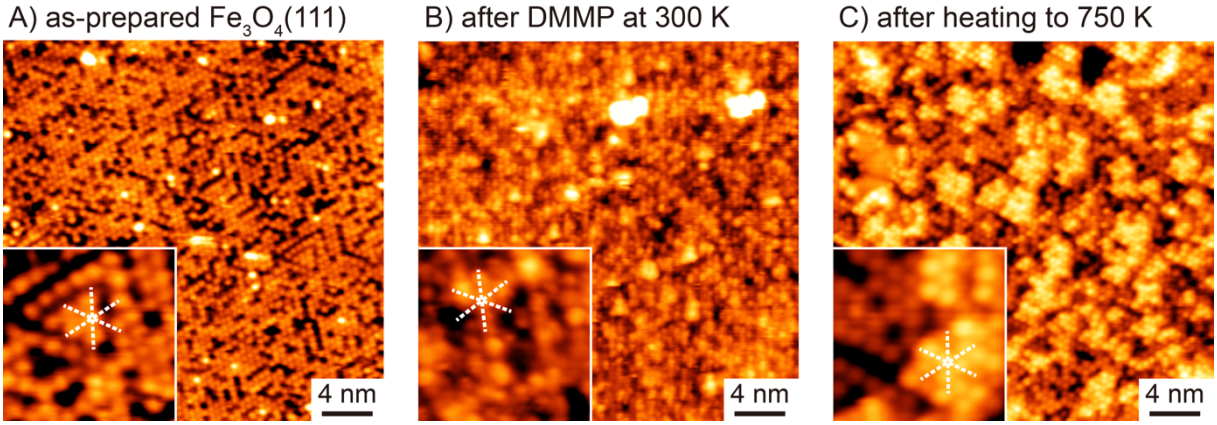

Fig. 4: Scanning tunneling microscope images show (A) the pristine $Fe_3O_4(111)$ thin film containing both O adatoms and tetrahedral coordinated lattice Fe; (B) short-range

ordered species are present after exposure to DMMP ($7.5x10^{-9}$ Torr for 60 s) at 300 K ; and, (C) formation of quasi-ordered P-containing islands formed after heating to 750 K to eliminate most C-containing species. The zoomed insets show an area of 5x5 nm^2 that illustrates the hexagonal packing in each case. The images were obtained at room temperature with a tunneling current of 0.02 nA and a bias of -2.2 V.

Successive DMMP Reaction Cycles

Island formation renders the surface sites accesbile again upon annealing to 750 K as is evident in the STM images (Fig. 4). Accordingly, multiple cycles of DMMP decompostion in TPRS are observed (Fig. 5). Indeed, subsequent exposures of DMMP at room temperature after the first temperature programmed experiments yield the same reaction products. The same reaction products, albeit with lower yields, are observed upon multiple repeated exposure-reaction cycles (Fig. 5, Table 2).

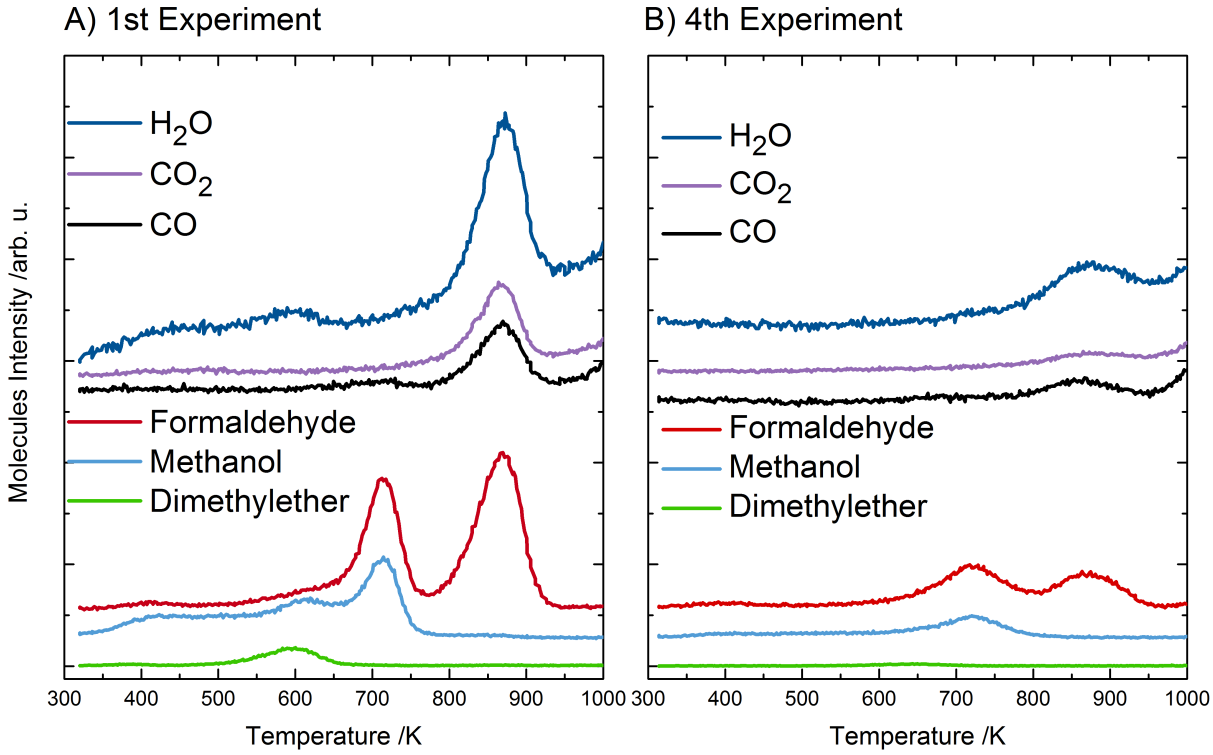

Fig. 5: Repeated cycles of temperature programmed reaction after exposure to DMMP at room temperature demonstrate that the residual POx species inhibit reaction but that activity persists for several cycles. Temperature programmed reaction data obtained after (A) exposure of the freshly-prepared $Fe_3O_4(111)/Fe_2O_3(0001)$ surface to DMMP at room temperature compared to data obtained after (B) the fourth consecutive exposure. All observed reaction products from the freshly prepared surface are also present in the 4^{th} cycle, but the yield is significantly diminished for all the observed molecules. The intensity scale is the same in both panels, but the traces are offset for clarity. The exposures used in each experiment were the same as that used to maximize product yields on the pristine surface. In each experiment, the surface was heated to 1000 K. The displayed masses are corrected for fragmentation and ionization and are the same as in Figure 1.

The presence of all products from the pristine $Fe_3O_4(111)/Fe_2O_3(0001)$ surface occurring at the same temperatures indicates that a certain amount of surface reaction sites are free. The reaction pathways are also unaltered by the presence of PO_x neighboring species. Just a minor change in the observed reaction channels is observed, since there is absolutely no water adsorbed on the surface in the following repeated exposures. This is illustrated best in the 4th cycle of DMMP reactions, where water desorbing from defects sites is not observed (no desorption up to 700 K) and consequently, also no methanol from the hydrolysis of methoxy species on the surface by surface hydroxyls occurs.

Tab. 2: Integrated molecule yields of the room temperature DMMP TPRS on a fresh surface and after multiple exposure-reaction cycles. The respective molecular yields are normalized to the on the pristine $Fe_3O_4(111)/Fe_2O_3(0001)$ surface.

TPD Run	Relative Integral Molecule Yield /%						
	DME	Methanol	CH_2O (720 K)	CH_2O (870 K)	CO	CO_2	H_2O
1	1.00	1.00	1.00	1.00	1.00	1.00	1.00
2	0.47	0.60	0.87	0.69	0.76	0.57	0.78
3	0.23	0.37	0.64	0.44	0.43	0.24	0.38
4	0.18	0.23	0.45	0.31	0.39	0.21	0.12

Probing Hydrolysis of DMMP

Despite the fact that hydrolysis is the major DMMP decomposition pathways at room temperature on metal organic frameworks[1, 54-56] or zirconium hydroxides,[1, 57-58] no additional reactivity due to water is observed. To probe the hydrolysis on the $Fe_3O_4(111)$ surface, the DMMP saturated surface was exposed to water at 300 K (4 L). No effect of exposure to water is observed during temperature programmed reaction of DMMP (Fig. 6A, 1)). When water is exposed to the surface prior to DMMP adsorption (Fig. 6B), distinct H_2O desorption features are observed at 400 K and 600 K. In analogy to previous studies of $Fe_3O_4(100)$,[59] these peaks are assigned to water or hydroxyls bound to defects. The high temperature water feature around 870 K is a result from the combustion of the residual phosphorous containing surface species and observed with similar intensities for all DMMP exposures, independent of H_2O adsorption.

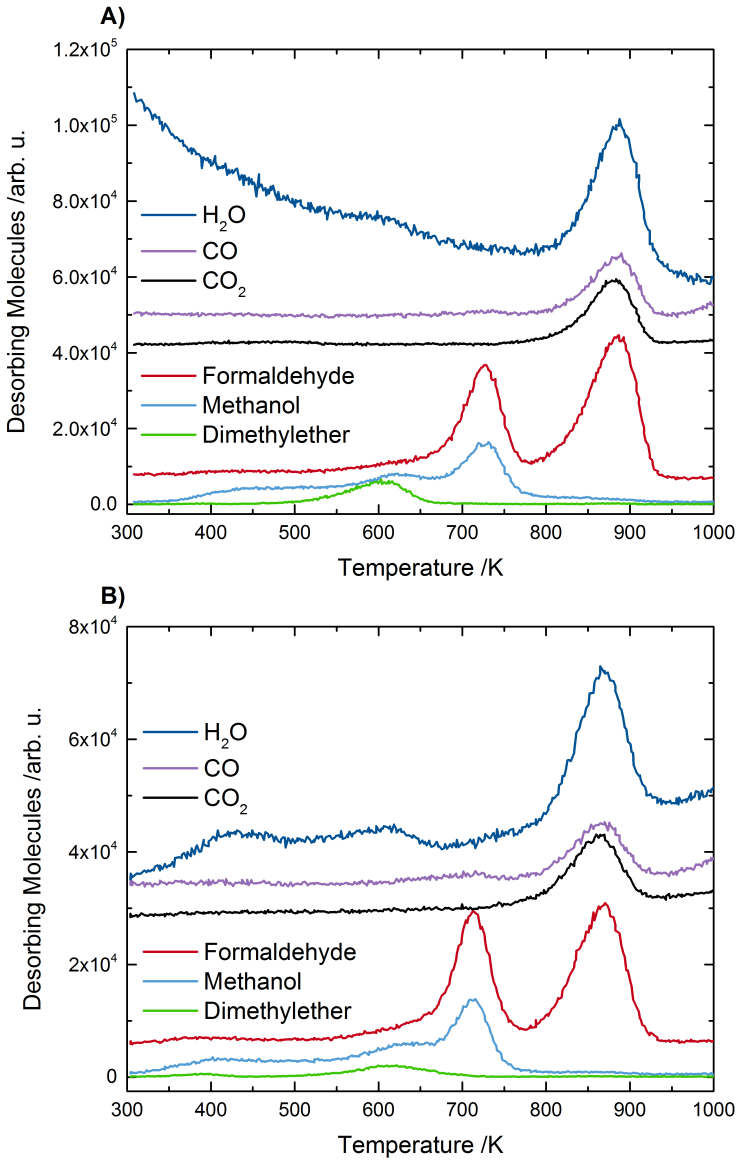

Fig. 6: Consecutive exposures of the $Fe_3O_4(111)/Fe_2O_3(0001)$ surface to DMMP and H_2O (A) and vice versa (B) at 300 K does not lead to significant hydrolysis as the reaction product distribution remains unaltered. The H_2O exposures are 10 min with a pressure of 2 $\times 10^{-10}$ Torr corresponding to a multilayer coverage. The displayed masses are corrected for fragmentation and ionization and are the same as in Figure 1.

Photoreactivity of DMMP

Illumination ($\lambda > 3.0$ eV, 10 mW/cm^2) of DMMP adsorbed on the n-type semiconductor hematite did not yield any detectable photochemical reaction products. Since bulk hematite is a semiconductor with an indirect band gap of 2.2 eV and direct band gap of 2.7 eV, illumination experiments with light above the band gap have been carried out with a DMMP saturated surface at room temperature. Light-assisted oxidation of DMMP has been envisioned as viable route to decompose DMMP thermally not accessible reaction pathways as shown i.e. on TiO_2-based light absorbers.[60-61] No product desorption is observed from the $Fe_3O_4(111)/Fe_2O_3(0001)$ surface (Fig. S13) upon illumination of the surface with light with energy above 3.0 eV. Temperature programmed after the illumination is the same with and without illumination (Figs. 1,

S14). Dissociative DMMP adsorption yields MMP and methoxy species on the surface, with the latter being commonly known as an efficient hole-scavenger.[62-63] In agreement with earlier work on stoichiometric Fe_2O_3(0001), photoreaction of methoxy species on the surface was not observed.[28] The lack of photochemical reactivity is most likely due to a short lifetime of the photohole[35], limited carrier diffusion lengths[64] and the absence of a (electro-)chemical bias.[65]

Comparison to other metal oxides

The decomposition of DMMP has been studied on various metal oxides and in agreement with a lot of other oxides,[7-9, 14-17, 21, 23-25, 52-53, 66] the major decomposition pathway on Fe_3O_4(111) is methoxy transfer to a metal cation surface site. Facile initial DMMP decomposition on the surface at room temperature, as evident from the reactivity studies (Figures 1 and S7), is important to eliminate the toxicity of the P-containing nerve agents or pesticides under ambient conditions. Further decomposition pathways apart from the methoxy transfer require higher reaction temperatures in agreement with previous studies on iron oxide powders.[7, 25, 67] Interestingly, the unique abilitiy of iron oxides to activate the P-CH_3 bond has been observed spectroscopically previously[25, 67] above room temperature in excellent agreement with the diemethyl ether formation from the MMP species on the Fe_3O_4(111) surface. Throughout all of the experiments, no desorption of phosphorous containing species was observed, which makes the reaction mechanism non-catalytic, since the P-species accumulate on the surface and the reactivity is diminished (Fig. 5). However, as a result, iron oxides might be very efficient at trapping DMMP at room temperature, since molecular desorption at 300 K and above has been observed for other oxides such as TiO_2(110)[19] and CeO_2(111)[22] and MoO_3.[17] The ability to trap the P-species on the surface and the absence of hydrolysis with water under the studied conditions may make magnetite materials very interesting for environmental clean-up reactions, since the trapping material can be separated from a matrix via its magnetic properties.[68]

Conclusion

Dimethyl methylphosphonate (DMMP), a model for toxic chemical warfare agents and pesticides, irreversibly dissociates on Fe_3O_4(111)/Fe_2O_3(0001) at room temperature to yield methoxy on Fe surface sites and methyl methylphosphonate (MMP) bound to oxygen adatoms. Further decomposition requires additional O adatoms migrating from the subsurface and temperatures above 600 K, yielding volatile organic oxygenates and strongly-bond PO_x. These residual PO_x species form islands as evidenced by STM, so reactivity on the surface towards DMMP decomposition persists through multiple exposures. In contrast to other materials such as zirconium hydroxides[1, 57-58], coadsorption of water and DMMP or its products does not lead to changes in reactivity, most likely due to the fact that water only weakly interacts with the surface at room temperature. Furthermore, illumination of the DMMP products does not lead to any

detectable photochemical reaction. Based on the observed surface chemistry, mesoporous structures of Fe_3O_4 or reductively treated Fe_2O_3 are promising candidates for new filter materials for a efficient decomposition of hazardous phosphonates.

Acknowledgments

We gratefully acknowledge support of this work by the U.S. Army Research Office under Grant No. W911NF1820143 and by the Defense Threat Reduction Agency under Program No. CB3934. This research used resources of the Center for Functional Nanomaterials, which is a U.S. DOE Office of Science Facility, at Brookhaven National Laboratory under Contract No. DE-SC0012704. The support of the staff at the Center for Function Nanomaterials (CFN), Brookhaven National Laboratories, especially Anibal Boscoboinik, is also acknowledged.

References

1. Kim, K.; Tsay, O. G.; Atwood, D. A.; Churchill, D. G., Destruction and Detection of Chemical Warfare Agents. *Chem. Rev.* **2011,** *111* (9), 5345-5403.
2. Head, A. R.; Trotochaud, L.; Tsyshevsky, R.; Fears, K.; Eichhorn, B.; Kuklja, M. M.; Bluhm, H., Coupling Ambient Pressure X-ray Photoelectron Spectroscopy with Density Functional Theory to Study Complex Surface Chemistry and Catalysis. *Top. Catal.* **2018,** *61* (20), 2175-2184.
3. Nowack, B., Environmental Chemistry of Phosphonates. *Water Res.* **2003,** *37* (11), 2533-2546.
4. Andreotti, G.; Koutros, S.; Hofmann, J. N.; Sandler, D. P.; Lubin, J. H.; Lynch, C. F.; Lerro, C. C.; De Roos, A. J.; Parks, C. G.; Alavanja, M. C.; Silverman, D. T.; Beane Freeman, L. E., Glyphosate Use and Cancer Incidence in the Agricultural Health Study. *J. Natl. Cancer Inst.* **2017,** *110* (5), 509-516.
5. Tarazona, J. V.; Court-Marques, D.; Tiramani, M.; Reich, H.; Pfeil, R.; Istace, F.; Crivellente, F., Glyphosate toxicity and carcinogenicity: a review of the scientific basis of the European Union assessment and its differences with IARC. *Arch. Toxicol.* **2017,** *91* (8), 2723-2743.
6. Parkinson, G. S., Iron Oxide Surfaces. *Surf. Sci. Rep.* **2016,** *71* (1), 272-365.
7. Sheinker, V. N.; Mitchell, M. B., Quantitative Study of the Decomposition of Dimethyl Methylphosphonate (DMMP) on Metal Oxides at Room Temperature and Above. *Chem. Mater.* **2002,** *14* (3), 1257-1268.
8. Mitchell, M. B.; Sheinker, V. N.; Cox, W. W., Room Temperature Reaction of Ozone and Dimethyl Methylphosphonate (DMMP) on Alumina-Supported Iron Oxide. *J. Phys. Chem. C* **2007,** *111* (26), 9417-9426.
9. Henderson, M. A.; Jin, T.; White, J. M., A TPD/AES study of the interaction of dimethyl methylphosphonate with iron oxide (.alpha.-Fe2O3) and silicon dioxide. *J. Phys. Chem.* **1986,** *90* (19), 4607-4611.
10. Woo, G. T.; Cha, J. B.; Kim, D. Y.; Seo, O. H., Positive Effects of Impregnation of Fe-oxide in Mesoporous Al-Oxides on the Decontamination of Dimethyl Methylphosphonate. *Catalysts* **2019,** *9* (11).

11. Henderson, M. A., Surface Chemistry of Trimethyl Phosphate on α-Fe2O3. *J. Phys. Chem. C* **2011,** *115* (47), 23527--23534.
12. Mäkie, P.; Westin, G.; Persson, P.; Österlund, L., Adsorption of Trimethyl Phosphate on Maghemite, Hematite, and Goethite Nanoparticles. *J. Phys. Chem. A* **2011,** *115* (32), 8948-8959.
13. Mäkie, P.; Persson, P.; Österlund, L., Adsorption of trimethyl phosphate and triethyl phosphate on dry and water pre-covered hematite, maghemite, and goethite nanoparticles. *J. Colloid Interface Sci.* **2013,** *392*, 349-358.
14. Trotochaud, L.; Tsyshevsky, R.; Holdren, S.; Fears, K.; Head, A. R.; Yu, Y.; Karslıoğlu, O.; Pletincx, S.; Eichhorn, B.; Owrutsky, J.; Long, J.; Zachariah, M.; Kuklja, M. M.; Bluhm, H., Spectroscopic and Computational Investigation of Room-Temperature Decomposition of a Chemical Warfare Agent Simulant on Polycrystalline Cupric Oxide. *Chem. Mater.* **2017,** *29* (17), 7483-7496.
15. Trotochaud, L.; Head, A. R.; Büchner, C.; Yu, Y.; Karslıoğlu, O.; Tsyshevsky, R.; Holdren, S.; Eichhorn, B.; Kuklja, M. M.; Bluhm, H., Room temperature decomposition of dimethyl methylphosphonate on cuprous oxide yields atomic phosphorus. *Surf. Sci.* **2019,** *680*, 75-87.
16. Gordon, W. O.; Tissue, B. M.; Morris, J. R., Adsorption and Decomposition of Dimethyl Methylphosphonate on Y2O3 Nanoparticles. *J. Phys. Chem. C* **2007,** *111* (8), 3233-3240.
17. Head, A. R.; Tang, X.; Hicks, Z.; Wang, L.; Bleuel, H.; Holdren, S.; Trotochaud, L.; Yu, Y.; Kyhl, L.; Karslıoğlu, O.; Fears, K.; Owrutsky, J.; Zachariah, M.; Bowen, K. H.; Bluhm, H., Thermal Desorption of Dimethyl Methylphosphonate from MoO3. *Catal. Struct. React.* **2017,** *3* (1-2), 112-118.
18. Rusu, C. N.; Yates, J. T., Adsorption and Decomposition of Dimethyl Methylphosphonate on TiO2. *J. Phys. Chem. B* **2000,** *104* (51), 12292-12298.
19. Ratliff, J. S.; Tenney, S. A.; Hu, X.; Conner, S. F.; Ma, S.; Chen, D. A., Decomposition of Dimethyl Methylphosphonate on Pt, Au, and Au−Pt Clusters Supported on TiO2(110). *Langmuir* **2009,** *25* (1), 216-225.
20. Panayotov, D. A.; Morris, J. R., Thermal Decomposition of a Chemical Warfare Agent Simulant (DMMP) on TiO2: Adsorbate Reactions with Lattice Oxygen as Studied by Infrared Spectroscopy. *J. Phys. Chem. C* **2009,** *113* (35), 15684-15691.
21. Holdren, S.; Tsyshevsky, R.; Fears, K.; Owrutsky, J.; Wu, T.; Wang, X.; Eichhorn, B. W.; Kuklja, M. M.; Zachariah, M. R., Adsorption and Destruction of the G-Series Nerve Agent Simulant Dimethyl Methylphosphonate on Zinc Oxide. *ACS Catal.* **2019,** *9* (2), 902-911.
22. Chen, D. A.; Ratliff, J. S.; Hu, X.; Gordon, W. O.; Senanayake, S. D.; Mullins, D. R., Dimethyl Methylphosphonate Decomposition on Fully Oxidized and Partially Reduced Ceria Thin Hilms. *Surf. Sci.* **2010,** *604* (5), 574-587.
23. Segal, S. R.; Cao, L.; Suib, S. L.; Tang, X.; Satyapal, S., Thermal Decomposition of Dimethyl Methylphosphonate over Manganese Oxide Catalysts. *J. Catal.* **2001,** *198* (1), 66-76.
24. Cao, L.; Segal, S. R.; Suib, S. L.; Tang, X.; Satyapal, S., Thermocatalytic Oxidation of Dimethyl Methylphosphonate on Supported Metal Oxides. *J. Catal.* **2000,** *194* (1), 61-70.
25. Mitchell, M. B.; Sheinker, V. N.; Mintz, E. A., Adsorption and Decomposition of Dimethyl Methylphosphonate on Metal Oxides. *J. Phys. Chem. B* **1997,** *101* (51), 11192-11203.
26. Fang Xu, W. C., Constantin A. Walenta, Christopher R. O'Connor, Cynthia M. Friend, Dual Lewis Site Creation for Activation of Methanol on Fe_3O_4(111) Thin Films. *Chem. Sci.* **2020**.

27. Crampton, A. S.; Cai, L.; Janvelyan, N.; Zheng, X.; Friend, C. M., Methanol Photo-Oxidation on Rutile TiO_2 Nanowires: Probing Reaction Pathways on Complex Materials. *J. Phys. Chem. C* **2017,** *121* (18), 9910-9919.
28. Walenta, C. A.; Crampton, A. S.; Xu, F.; Heiz, U.; Friend, C. M., Chemistry of Methanol and Ethanol on Ozone-Prepared α-Fe_2O_3(0001). *J. Phys. Chem. C* **2018,** *122* (44), 25404-25410.
29. Kuhlenbeck, H.; Shaikhutdinov, S.; Freund, H.-J., Well-Ordered Transition Metal Oxide Layers in Model Catalysis – A Series of Case Studies. *Chem. Rev.* **2013,** *113* (6), 3986-4034.
30. Genuzio, F.; Sala, A.; Schmidt, T.; Menzel, D.; Freund, H.-J., Interconversion of α-Fe2O3 and Fe3O4 Thin Films: Mechanisms, Morphology, and Evidence for Unexpected Substrate Participation. *J. Phys. Chem. C* **2014,** *118* (50), 29068-29076.
31. Smentkowski, V. S.; Hagans, P.; Yates, J. T., Study of the catalytic destruction of dimethyl methylphosphonate(DMMP): oxidation over molybdenum(110). *J. Phys. Chem.* **1988,** *92* (22), 6351-6357.
32. Harrison, A. G.; Jones, E. G.; Gupta, S. K.; Nagy, G. P., TOTAL CROSS SECTIONS FOR IONIZATION BY ELECTRON IMPACT. *Can. J. Chem.* **1966,** *44* (16), 1967-1973.
33. Gupta, D.; Antony, B., Electron Impact Ionization of Cycloalkanes, Aldehydes, and Ketones. *J. Chem. Phys.* **2014,** *141* (5), 054303.
34. Bull, J. N.; Harland, P. W.; Vallance, C., Absolute Total Electron Impact Ionization Cross-Sections for Many-Atom Organic and Halocarbon Species. *J. Phys. Chem. A* **2012,** *116* (1), 767-777.
35. Barroso, M.; Pendlebury, S. R.; Cowan, A. J.; Durrant, J. R., Charge Carrier Trapping, Recombination and Transfer in Hematite (α-Fe2O3) Water Splitting Photoanodes. *Chem. Sci.* **2013,** *4* (7), 2724-2734.
36. Xu, F.; Madix, R. J.; Friend, C. M., Spatially Nonuniform Reaction Rates during Selective Oxidation on Gold. *J. Am. Chem. Soc.* **2018,** *140* (38), 12210-12215.
37. Shirley, D. A., High-Resolution X-Ray Photoemission Spectrum of the Valence Bands of Gold. *Phys. Rev. B* **1972,** *5* (12), 4709-4714.
38. Bomben, J. F. M. W. F. S. P. E. S. K. D., *Handbook of X-Ray Photoelectron Spectroscopy*. Perkin Elmer Corporation Physical Electronics Division: 6509 Flying Cloud Drive, Eden Prairie, Minnesota 55344, United States of America, 1992.
39. Kresse, G.; Furthmüller, J., Efficient Iterative Schemes for ab initio Total-Energy Calculations using a Plane-Wave Basis Set. *Phys. Rev. B* **1996,** *54* (16), 11169-11186.
40. Kresse, G.; Joubert, D., From Ultrasoft Pseudopotentials to the Projector Augmented-Wave Method. *Phys. Rev. B* **1999,** *59* (3), 1758-1775.
41. Perdew, J. P.; Burke, K.; Ernzerhof, M., Generalized Gradient Approximation Made Simple. *Phys. Rev. Lett.* **1996,** *77* (18), 3865-3868.
42. Steinmann, S. N.; Corminboeuf, C., A generalized-gradient approximation exchange hole model for dispersion coefficients. *J. Chem. Phys.* **2011,** *134* (4), 044117.
43. Steinmann, S. N.; Corminboeuf, C., Comprehensive Benchmarking of a Density-Dependent Dispersion Correction. *J. Chem. Theory Comput.* **2011,** *7* (11), 3567-3577.
44. Zaki, E.; Jakub, Z.; Mirabella, F.; Parkinson, G. S.; Shaikhutdinov, S.; Freund, H.-J., Water Ordering on the Magnetite Fe3O4 Surfaces. *J. Phys. Chem. Lett.* **2019**, 2487-2492.
45. Makov, G.; Payne, M. C., Periodic boundary conditions in ab initio calculations. *Phys. Rev. B* **1995,** *51* (7), 4014-4022.

46. Dudarev, S. L.; Botton, G. A.; Savrasov, S. Y.; Humphreys, C. J.; Sutton, A. P., Electron-Energy-Loss Spectra and the Structural Stability of Nickel Oxide: An LSDA+U Study. *Phys. Rev. B* **1998,** *57* (3), 1505-1509.
47. Łodziana, Z., Surface Verwey Transition in Magnetite. *Phys. Rev. Lett.* **2007,** *99* (20), 206402.
48. Jeng, H.-T.; Guo, G. Y.; Huang, D. J., Charge-orbital ordering in low-temperature structures of magnetite: $\mathrm{GGA}+U$ investigations. *Phys. Rev. B* **2006,** *74* (19), 195115.
49. Monkhorst, H. J.; Pack, J. D., Special points for Brillouin-zone integrations. *Phys. Rev. B* **1976,** *13* (12), 5188-5192.
50. Li, X.; Paier, J., Partial Oxidation of Methanol on the Fe3O4(111) Surface Studied by Density Functional Theory. *J. Phys. Chem. C* **2019,** *123* (13), 8429-8438.
51. Ma, S.; Zhou, J.; Kang, Y. C.; Reddic, J. E.; Chen, D. A., Dimethyl Methylphosphonate Decomposition on Cu Surfaces: Supported Cu Nanoclusters and Films on TiO2(110). *Langmuir* **2004,** *20* (22), 9686-9694.
52. Tang, X.; Hicks, Z.; Ganteför, G.; Eichhorn, B. W.; Bowen, K. H., Adsorption and Decomposition of DMMP on Size-Selected (WO3)3 Clusters. *ChemistrySelect* **2018,** *3* (13), 3718-3721.
53. Tang, X.; Hicks, Z.; Wang, L.; Ganteför, G.; Bowen, K. H.; Tsyshevsky, R.; Sun, J.; Kuklja, M. M., Adsorption and decomposition of dimethyl methylphosphonate on size-selected (MoO3)3 clusters. *Phys. Chem. Chem. Phys.* **2018,** *20* (7), 4840-4850.
54. Wang, G.; Sharp, C.; Plonka, A. M.; Wang, Q.; Frenkel, A. I.; Guo, W.; Hill, C.; Smith, C.; Kollar, J.; Troya, D.; Morris, J. R., Mechanism and Kinetics for Reaction of the Chemical Warfare Agent Simulant, DMMP(g), with Zirconium(IV) MOFs: An Ultrahigh-Vacuum and DFT Study. *The Journal of Physical Chemistry C* **2017,** *121* (21), 11261-11272.
55. Bobbitt, N. S.; Mendonca, M. L.; Howarth, A. J.; Islamoglu, T.; Hupp, J. T.; Farha, O. K.; Snurr, R. Q., Metal–organic frameworks for the removal of toxic industrial chemicals and chemical warfare agents. *Chem. Soc. Rev.* **2017,** *46* (11), 3357-3385.
56. Liu, Y.; Howarth, A. J.; Vermeulen, N. A.; Moon, S.-Y.; Hupp, J. T.; Farha, O. K., Catalytic Degradation of Chemical Warfare Agents and Their Simulants by Metal-Organic Frameworks. *Coord. Chem. Rev.* **2017,** *346*, 101-111.
57. Tian, Y.; Plonka, A. M.; Ebrahim, A. M.; Palomino, R. M.; Senanayake, S. D.; Balboa, A.; Gordon, W. O.; Troya, D.; Musaev, D. G.; Morris, J. R.; Mitchell, M. B.; Collins-Wildman, D. L.; Hill, C. L.; Frenkel, A. I., Correlated Multimodal Approach Reveals Key Details of Nerve-Agent Decomposition by Single-Site Zr-Based Polyoxometalates. *J. Phys. Chem. Lett.* **2019,** *10* (9), 2295-2299.
58. Jeon, S.; Schweigert, I. V.; Pehrsson, P. E.; Balow, R. B., Kinetics of Dimethyl Methylphosphonate Adsorption and Decomposition on Zirconium Hydroxide Using Variable Temperature In Situ Attenuated Total Reflection Infrared Spectroscopy. *ACS Appl. Mater. Interfac.* **2020**.
59. Meier, M.; Hulva, J.; Jakub, Z.; Pavelec, J.; Setvin, M.; Bliem, R.; Schmid, M.; Diebold, U.; Franchini, C.; Parkinson, G. S., Water Agglomerates on Fe3O4(001). *Proc. Natl. Acad. Sci.* **2018,** *115* (25), E5642.
60. Kozlova, E. A.; Vorontsov, A. V., Photocatalytic hydrogen evolution from aqueous solutions of organophosphorous compounds. *International Journal of Hydrogen Energy* **2010,** *35* (14), 7337-7343.
61. Rusu, C. N.; Yates, J. T., Photooxidation of Dimethyl Methylphosphonate on TiO2 Powder. *The Journal of Physical Chemistry B* **2000,** *104* (51), 12299-12305.

62. Shen, M.; Henderson, M. A., Identification of the Active Species in Photochemical Hole Scavenging Reactions of Methanol on TiO_2. *J. Phys. Chem. Lett.* **2011,** *2* (21), 2707-2710.
63. Schneider, J.; Matsuoka, M.; Takeuchi, M.; Zhang, J.; Horiuchi, Y.; Anpo, M.; Bahnemann, D. W., Understanding TiO2 Photocatalysis: Mechanisms and Materials. *Chem. Rev.* **2014,** *114* (19), 9919-9986.
64. Bora, D. K.; Braun, A.; Constable, E. C., "In rust we trust". Hematite - The Prospective Inorganic Backbone for Artificial Photosynthesis. *Energy Environ. Sci.* **2013,** *6* (2), 407-425.
65. Klahr, B.; Gimenez, S.; Zandi, O.; Fabregat-Santiago, F.; Hamann, T., Competitive Photoelectrochemical Methanol and Water Oxidation with Hematite Electrodes. *ACS Appl. Mat. Interfaces* **2015,** *7* (14), 7653-7660.
66. Head, A. R.; Tsyshevsky, R.; Trotochaud, L.; Yu, Y.; Karslıoğlu, O.; Eichhorn, B.; Kuklja, M. M.; Bluhm, H., Dimethyl Methylphosphonate Adsorption and Decomposition on MoO2 as Studied by Ambient Pressure X-Ray Photoelectron Spectroscopy and DFT Calculations. *J. Phys.: Condens. Matter* **2018,** *30* (13), 134005.
67. Tesfai, T. M.; Sheinker, V. N.; Mitchell, M. B., Decomposition of Dimethyl Methylphosphonate (DMMP) on Alumina-Supported Iron Oxide. *J. Phys. Chem. B* **1998,** *102* (38), 7299-7302.
68. Cundy, A. B.; Hopkinson, L.; Whitby, R. L. D., Use of Iron-Based Technologies in Contaminated Land and Groundwater Remediation: A Review. *Sci. Tot. Env.* **2008,** *400* (1), 42-51.

Table of Contents Graphic: